frontiers | Frontiers in Medicine

TYPE Original Research
PUBLISHED 13 August 2024
DOI 10.3389/fmed.2024.1447500



OPEN ACCESS

EDITED BY
Chuangyan Zhai,
Southern Medical University, China

REVIEWED BY
Shaoyu Liu,
First Affiliated Hospital of Guangzhou Medical University, China
Penghui Sun,
Southern Medical University, China

*CORRESPONDENCE
Xun Wang
✉ 081104125@fudan.edu.cn

RECEIVED 11 June 2024
ACCEPTED 30 July 2024
PUBLISHED 13 August 2024

CITATION
Li S, Wang K, Zhu X, Pan D, Wang L, Guo X, Gao X, Luo Q and Wang X (2024) The diagnostic value of $^{68}$Ga-NOTA-MAL-Cys-MZHER$_{2:342}$ PET/CT imaging for HER2-positive lung adenocarcinoma.
*Front. Med.* 11:1447500.
doi: 10.3389/fmed.2024.1447500



# The diagnostic value of $^{68}$Ga-NOTA-MAL-Cys-MZHER$_{2:342}$ PET/CT imaging for HER2-positive lung adenocarcinoma

Shu Li[1,2], Ke Wang[3], Xue Zhu[3], Donghui Pan[3], Ling Wang[3], Xu Guo[4], Xiaomin Gao[2,4], Qing Luo[2,4] and Xun Wang[1,2,5]*

[1]Department of Pulmonary and Critical Care Medicine, Jiangnan University Medical Center, Jiangnan University (Wuxi No. 2 People's Hospital), Wuxi, Jiangsu, China, [2]Wuxi School of Medicine, Jiangnan University, Wuxi, Jiangsu, China, [3]NHC Key Laboratory of Nuclear Medicine, Jiangsu Key Laboratory of Molecular Nuclear Medicine, Jiangsu Institute of Nuclear Medicine, Wuxi, Jiangsu, China, [4]Wuxi Maternity and Child Health Care Hospital, Affiliated Women's Hospital of Jiangnan University, Wuxi, Jiangsu, China, [5]Nantong University Medical School, Nantong, Jiangsu, China

**Background:** The human epidermal growth factor receptor 2 gene (HER2) has been identified as a potential therapeutic target in lung adenocarcinoma (LUAD). Non-invasive positron emission tomography (PET) imaging provides a reliable strategy for *in vivo* determination of HER2 expression through whole-body detection of abnormalities. The PET tracer $^{68}$Ga-NOTA-MAL-Cys-MZHER$_{2:342}$ has shown promising results for HER2-positive breast and gastric cancers. This study aims to evaluate the performance of $^{68}$Ga-NOTA-MAL-Cys-MZHER$_{2:342}$ *in vitro* and *in vivo* models and in clinical patients with HER2-positive LUAD.

**Methods:** NOTA-MAL-Cys-MZHER$_{2:342}$ was synthesized and labeled with $^{68}$Ga. Cell uptake, cell binding ability, and stability studies of $^{68}$Ga-NOTA-MAL-Cys-MZHER$_{2:342}$ were assessed both in the Calu-3 lung cancer (LC) cell line and normal mice. *In vivo* assessment in tumor-bearing mice was conducted using microPET imaging and biodistribution experiments. Additionally, preliminary PET/CT imaging analysis was performed on HER2-positive LC patients.

**Results:** $^{68}$Ga-NOTA-MAL-Cys-MZHER$_{2:342}$ was prepared with a radiochemical purity (RCP) exceeding 95%. The tracer demonstrated high cell uptake in HER2-overexpressing Calu-3 cells, with an $IC_{50}$ of 158.9, an adequate 1.73 nM. Good stability was exhibited both *in vitro* and *in vivo*. MicroPET imaging of Calu-3-bearing mice revealed high tumor uptake and notable tumor-to-background ratios. Positive outcomes were also observed in two HER2-positive LUAD patients.

**Conclusion:** $^{68}$Ga-NOTA-MAL-Cys-MZHER$_{2:342}$ demonstrated satisfactory stability, sensitivity, and specificity. These findings suggest that $^{68}$Ga-NOTA-MAL-Cys-MZHER$_{2:342}$ PET/CT imaging provides a novel tool for non-invasive visual assessment of HER2 expression in LUAD patients.

KEYWORDS

$^{68}$Ga-NOTA-MAL-Cys-MZHER2:342, $^{18}$F-FDG, PET, lung cancer, HER2

# Introduction

LC has emerged as the leading cause of malignant tumor-related mortality worldwide, accounting for 1.8 million deaths annually (1–3). Adenocarcinoma, comprising approximately 40% of all LC cases, represents the most prevalent subtype. The implementation of molecular targeted therapy has significantly improved the overall prognosis and quality of life for patients with LUAD. However, the absence of effective targeted agents for numerous driver mutations underscores the necessity for novel therapeutic approaches. Among these genetic alterations, human epidermal growth factor receptor 2 (HER2/ERBB2) mutations are observed in 2–3% of LUAD cases (4, 5). HER2 alterations, encompassing mutations, amplifications, and overexpression, are associated with aggressive tumor growth and elevated metastasis rates. Furthermore, acquired HER2 amplification has been proposed as a mechanism of resistance to EGFR/ALK tyrosine kinase inhibitors (TKIs), further substantiating its role in tumorigenesis (6, 7). Recent years have witnessed the emergence of novel compounds, such as trastuzumab deruxtecan (T-DXd, DS-8201) and poziotinib, which have increased the objective response rate (ORR) to approximately 50% for patients with HER2-positive LUAD (8, 9). Consequently, the detection of HER2 status in LUAD has become crucial for developing and selecting appropriate treatment regimens.

Current diagnostic methods for HER2-positive cancer primarily rely on fluorescence *in situ* hybridization (FISH) and immunohistochemistry (IHC) (10). While these techniques yield relatively clear results for tumors with absent or overexpressed HER2, accurately quantifying HER2 in tumors with moderate expression remains challenging (11). PET, a three-dimensional molecular imaging modality utilizing radioisotopes, has demonstrated significant clinical value in cancer diagnosis (12, 13). $^{18}$F-fluorodeoxyglucose positron emission tomography-computed tomography ($^{18}$F-FDG PET/CT) is currently the most widely employed tracer in clinical practice. However, this approach primarily assesses tumor metabolic activity rather than detecting the status of driver genes (14, 15). To develop a non-invasive method for predicting which cancer patients will benefit from HER2-targeted therapy, extensive research has focused on developing PET tracers targeting this receptor. $^{64}$Cu-DOTA-trastuzumab, derived from trastuzumab, has shown promising results *in vitro* and *in vivo* for detecting HER2-positive lung and breast cancers (16, 17). $^{99m}$Tc-$Z_{HER2:V2}$-pemetrexed enables precise visualization and treatment in a HER2-positive (A549) xenograft model through the combination of HER2 affinity and pemetrexed (18, 19). Moreover, the $ZHER_{2:342}$ Affibody conjugated with N-[2-(4-$^{18}$F-fluorobenzamido)ethyl]maleimide has demonstrated specificity in evaluating HER2 expression *in vivo* and in breast cancer metastasis models (20, 21). However, complex synthesis procedures, lower RCP, and prolonged targeting times have limited their clinical application. Previous research has demonstrated that the hydrophilic linker (GGGRDN)-modified $ZHER_{2:342}$ affibody ($MZHER_{2:342}$), when coupled with maleimide-NOTA (MAL-NOTA), yields a conjugate that exhibits notable tumor-to-background ratios following labeling with $^{18}$FAl/$^{68}$Ga (22–25). To date, clinical studies on HER2-targeted tracers in LUAD remain scarce. The present study aims to investigate the efficacy of the HER2 affibody tracer $^{68}$Ga-NOTA-MAL-Cys-$MZHER_{2:342}$ for PET imaging of HER2-positive LUAD and compare its performance with that of $^{18}$F-FDG.

# Materials and methods

## General materials

Fluorodeoxyglucose (FDG) was supplied by Wuxi Jiangyuan Industrial Technology and Trade Corporation, China. Cys-$MZHER_{2:342}$ was synthesized by Shanghai Apeptide Biotechnology Corporation, China. NOTA-MAL-Cys-$MZHER_{2:342}$ was prepared following established methods, achieving a chemical purity exceeding 95% (25). The $^{68}$Ge/$^{68}$Ga generator was procured from Isotope Technologies Garching (ITG), Germany. All other reagents utilized were of analytical grade.

## Preparation of $^{68}$Ga-NOTA-MAL-Cys-$MZHER_{2:342}$

NOTA-MAL-Cys-$MZHER_{2:342}$ (150 μg, 25 nmol) was dissolved in 30 μL of deionized water. Subsequently, $^{68}GaCl_3$ eluent (185 MBq, 2 mL) and 1 M sodium acetate solution (120 μL) were added, maintaining a pH range of 3–3.5. The resulting mixture was heated in an oil bath at 70°C for 10 min. Following heating, the mixture was diluted with 8 mL of deionized water and transferred to an activated BOND ELUT C18 column (Varian Medical Systems, United States). Impurities removed by washing with 10 mL of deionized water. The product was then eluted using 0.3 mL of 10 mM HCl ethanol. The eluent was further diluted with 5 mL of saline and filtered through a 0.22 μm Millipore filter into a sterile vial. RCP was assessed using high-performance liquid chromatography (HPLC, Waters, United States) in accordance with previously established protocols (24, 26).

## Cell lines and culture

The human LC cell lines Calu-3 and NCI-H520 were obtained from the Cell Bank of Shanghai Institutes for Biological Sciences, China. These cell lines were cultured in RPMI-1640 medium supplemented with 10% fetal bovine serum (FBS, Gibco Life Technologies, United States) and 1% penicillin–streptomycin (P-S) solution. The culture conditions were maintained at 37°C in a humidified atmosphere containing 5% $CO_2$.

## Cell uptake and block studies

For the cell uptake assay, Calu-3 (HER2-positive) and NCI-H520 (HER2-negative) cells were seeded in 12-well plates at a density of $1 \times 10^6$ cells per well and cultured overnight. After washing with PBS, the cells were incubated with 370 KBq of $^{68}$Ga-NOTA-MAL-Cys-$MZHER_{2:342}$ at 37°C in a 5% $CO_2$ environment for 15, 30, 60, and 120 min, respectively. In the cell block study, sufficient quantities of unlabeled Cys-$MZHER_{2:342}$ (1 μM) were added to the 12-well plates and incubated for 10 min prior to re-incubation with $^{68}$Ga-NOTA-MAL-Cys-$MZHER_{2:342}$ for various durations. Following incubation, the cells were washed with ice-cold PBS and lysed with 1 mL of NaOH (1 M) for 1 min. The lysate was transferred to γ-counting tubes and measured using a γ counter (Perkin Elmer Instruments Corporation, United States). Cell uptake was expressed as a percentage of decay-corrected radiation dose per counting tube (%AD/$10^5$ cells).

## Cell binding assay

For the cell binding assay, Calu-3 cells were seeded in 24-well plates at a density of $1 \times 10^5$ cells per well and cultured overnight. After washing with PBS, the cells were incubated with 370 KBq of $^{68}$Ga-NOTA-MAL-Cys-MZHER$_{2:342}$ in conjunction with varying concentrations of unlabeled Cys-MZHER$_{2:342}$ peptide. Following a 2-h incubation period, the cells were washed with ice-cold PBS and lysed by adding 1 M NaOH for 1 min. The resulting lysate was transferred to γ-counting tubes and measured using a γ counter. The 50% inhibitory concentration ($IC_{50}$) value was calculated using GraphPad Prism 8.0 software (San Diego, United States).

## Stability analysis

The stability of $^{68}$Ga-NOTA-MAL-Cys-MZHER$_{2:342}$ was evaluated through *in vitro* and *in vivo* experiments. For *in vitro* stability, 3.7 MBq of the radiotracer was incubated with FBS or phosphate-buffered saline (PBS) at 37°C. The RCP was analyzed by HPLC at 15, 30, 60, and 120 min. *In vivo* stability was assessed in normal male mice (4 weeks old, Changzhou Cavins Laboratory Animals Ltd., China). These mice were administered 37 MBq of $^{68}$Ga-NOTA-MAL-Cys-MZHER$_{2:342}$ via tail vein injection. Blood samples were collected in heparinized centrifuge tubes at 15-, 30-, and 60-min post-injection. The collected blood was immediately centrifuged at 10,000 rpm for 3 min. Protein precipitation was achieved by adding 500 μL of acetonitrile to the resulting plasma. The mixture was subsequently centrifuged at 9,000 rpm for 5 min to obtain the supernatant. The supernatant was filtered through a microporous membrane and subjected to HPLC analysis.

## *In vivo* microPET imaging

Male BALB/c nude mice (4 weeks old, Changzhou Cavins Laboratory Animals Ltd., China) were utilized for *in vivo* microPET imaging. Calu-3 cells ($5 \times 10^5$) were subcutaneously injected into these mice. Subsequent experiments were conducted when the tumor size reached approximately 300 cubic millimeters (10 days post-injection). For imaging, mice received a tail vein injection of 100 μL of $^{68}$Ga-NOTA-MAL-Cys-MZHER$_{2:342}$ (3.7 MBq). Static PET images were acquired for 10 min at 1-h post-injection ($n = 4$ per group). Blocking experiments were performed by co-injecting an excess amount of unlabeled Cys-MZHER$_{2:342}$ with the labeled $^{68}$Ga-NOTA-MAL-Cys-MZHER$_{2:342}$ into Calu-3-bearing mice. A 10-min static PET scan was conducted 1-h post-injection. Quantitative analysis of PET images was performed according to previously reported methods (27). Animal experiments were approved by the Animal Research Committee of Jiangsu Institute of Atomic Medicine (JSINM-2022-061).

## *Ex vivo* biodistribution analysis

Mice bearing Calu-3 tumors were injected with approximately 740 KBq of radiolabeled $^{68}$Ga-NOTA-MAL-Cys-MZHER$_{2:342}$. These mice were euthanized at predetermined time points. Blood, tumors, and major organs were harvested and weighed. Radioactivity measurements were conducted using a gamma counter. The data were calculated and expressed as a percentage of the injected dose per gram of tissue (%ID/g).

## Clinical patients and PET imaging

This clinical study was approved by the Ethics Committee of the Peking University Cancer Hospital (NCT04547309). This study included two LUAD patients without severe hepatic or renal dysfunction. All patients provided written informed consent. PET/CT scans were performed using a Biograph 64 PET/CT scanner (Siemens Medical Solutions, Nuremberg, Germany). Following the injection of 74 MBq of $^{68}$Ga-NOTA-MAL-Cys-MZHER$_{2:342}$, patients were positioned supine on the scanning bed. Dynamic scans were conducted for 60 min, covering the brain and whole-body regions. PET images were reconstructed using three-dimensional ordered-subset expectation maximization. Biodistribution analysis was performed using PET images. Regions of interest (ROIs) for the tumor and major organs (e.g., brain, lung, heart, liver, spleen, and kidney) were delineated with the assistance of corresponding CT images. Standardized uptake values (SUVs) were calculated according to previously described methods (22, 28).

## Histology and immunohistochemistry

Tumor tissues were surgically excised from each mouse and allowed to decay radioactively for over 48 h to ensure sufficiently reduced radioactivity levels. Subsequently, the tissues were fixed in formalin, embedded in paraffin, and sectioned. For immunohistochemical staining, the sections were incubated with HER2 antibody (ab134182, Rabbit mAb, Abcam, United States) overnight at 4°C, followed by a 2-h incubation with an HRP-conjugated secondary antibody at room temperature. Visualization of the sections was achieved using a DAB kit (Beyotime, China), and observations were made using a light microscope (Olympus IX53, Tokyo, Japan). HER2 expression levels were classified into four grades (0+ to 3+) based on the number and intensity of tumor cell membrane staining. HER2 expression in the tumor tissue was categorized as either positive (IHC: 2+ to 3+) or negative (IHC: 0+ to 1+).

## Statistical analysis

Statistical analyses were conducted using GraphPad Prism (v. 5.0, GraphPad software). Comparisons between groups were evaluated using the Student's *t*-test and one-way analysis of variance (ANOVA). Statistical significance was defined as a *p*-value of $<0.05$.

# Results

## Chemistry and radiochemistry

The conjugation of NOTA-MAL with Cys-MZHER$_{2:342}$ was performed at 40°C, resulting in the acquisition of NOTA-MAL-Cys-MZHER$_{2:342}$ with an approximate yield of 50%. An efficient $^{68}$Ga

labeling method was used for $^{68}$Ga-NOTA-MAL-Cys-MZHER$_{2:342}$. The probes were produced within 30 min with a yield of 62.53 ± 5.24% ($n$ = 3) (Figure 1A, based on $^{68}$Ga, non-decay-corrected). Analytical HPLC determined that the RCPs of the compounds exceeded 90% (Figure 1B).

## Cell uptake and binding assays and stability analysis

The cell uptake and block studies were conducted utilizing Calu-3 and NCI-H520 cell lines. As illustrated in Figure 2A, Calu-3 cells (HER2-positive) exhibited a cell uptake of 1.16 ± 0.01 %AD/10$^5$ cells after 60 min of incubation. This uptake was significantly reduced to 0.44 ± 0.04 %AD/10$^5$ cells ($n$ = 3, $p$ < 0.001) upon the addition of unlabeled Cys-MZHER$_{2:342}$. Conversely, NCI-H520 cells (HER2-negative) demonstrated a cell uptake of 0.71 ± 0.04 %AD/10$^5$ cells ($p$ < 0.001), which was comparable to the results obtained in the cell block assay. A competitive binding assay was subsequently performed. Figure 2B demonstrates that unlabeled Cys-MZHER$_{2:342}$ inhibited the binding of $^{68}$Ga-NOTA-MAL-Cys-MZHER$_{2:342}$ to Calu-3 cells in a dose-dependent manner, with an IC$_{50}$ of 158.9 ± 1.73 nM ($n$ = 3). *In vitro* stability analysis revealed that $^{68}$Ga-NOTA-MAL-Cys-MZHER$_{2:342}$ maintained stability at 37°C for a minimum of 2 h in both FBS and PBS solutions, retaining 95% purity after 2 h of incubation. Furthermore, the compound exhibited good stability 1-h post-injection *in vivo* (Figure 2C).

## MicroPET imaging and biodistribution studies

Following radiolabeling, microPET scans were conducted to assess the efficacy of $^{68}$Ga-NOTA-MAL-Cys-MZHER$_{2:342}$ in Calu-3-bearing mice. As depicted in Figure 3A, tumor uptake of $^{68}$Ga-NOTA-MAL-Cys-MZHER$_{2:342}$ (15.77 ± 2.13 %ID/g) was observed 60-min post-injection, resulting in favorable tumor-background ratios. One hour after co-injection with Cys-MZHER$_{2:342}$, the tumor signal was significantly reduced, with an uptake value of 2.73 ± 0.58 %ID/g. Notably, renal accumulation reached 103.4 ± 5.23 %ID/g at 1-h post-injection, substantially higher than in other normal tissues. This observation suggests that the tracer is primarily excreted through the renal system. Figure 3B and Table 1 illustrate the biodistribution of $^{68}$Ga-NOTA-MAL-Cys-MZHER$_{2:342}$ in Calu-3-bearing mice. The tumor uptake was 16.11 ± 3.91 %ID/g, while uptake in the heart, liver, lung, and kidney was 0.5 ± 0.03, 3.55 ± 0.73, 2.44 ± 1.07, and 106.85 ± 0.61 %ID/g, respectively ($n$ = 3). The tumor-to-blood and tumor-to-muscle uptake ratios were calculated to be 24.29 ± 1.93 and 35.77 ± 2.14, respectively. HER2 expression in tumor tissues was further evaluated through immunohistochemical assays, which revealed high expression levels (Figure 3C).

## PET imaging of clinical patients

PET/CT imaging was conducted on two HER2-positive LUAD patients using $^{18}$F-FDG and $^{68}$Ga-NOTA-MAL-Cys-MZHER$_{2:342}$. As

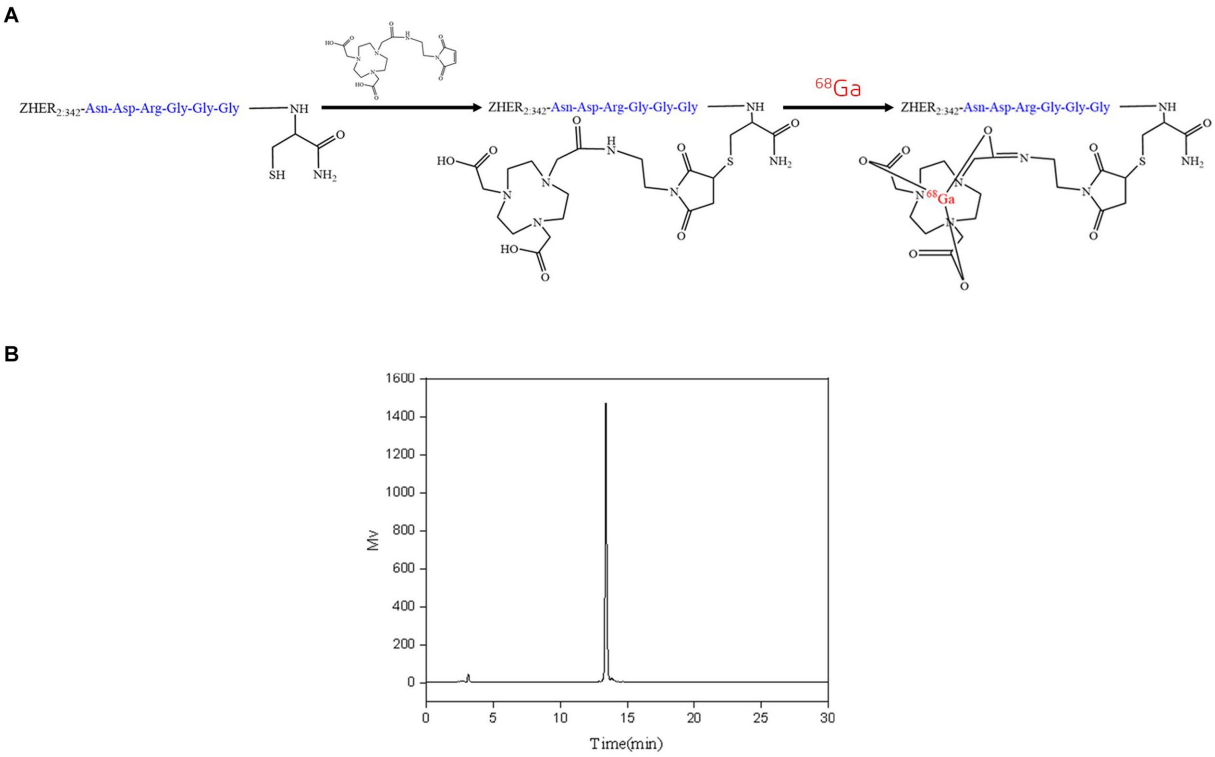


FIGURE 1
Radiolabeling of NOTA-MAL-Cys-MZHER$_{2:342}$. **(A)** Synthetic methodology for $^{68}$Ga-NOTA-MAL-Cys-MZHER$_{2:342}$. **(B)** High-performance liquid chromatography (HPLC) detection of $^{68}$Ga-NOTA-MAL-Cys-MZHER$_{2:342}$ radioactivity.

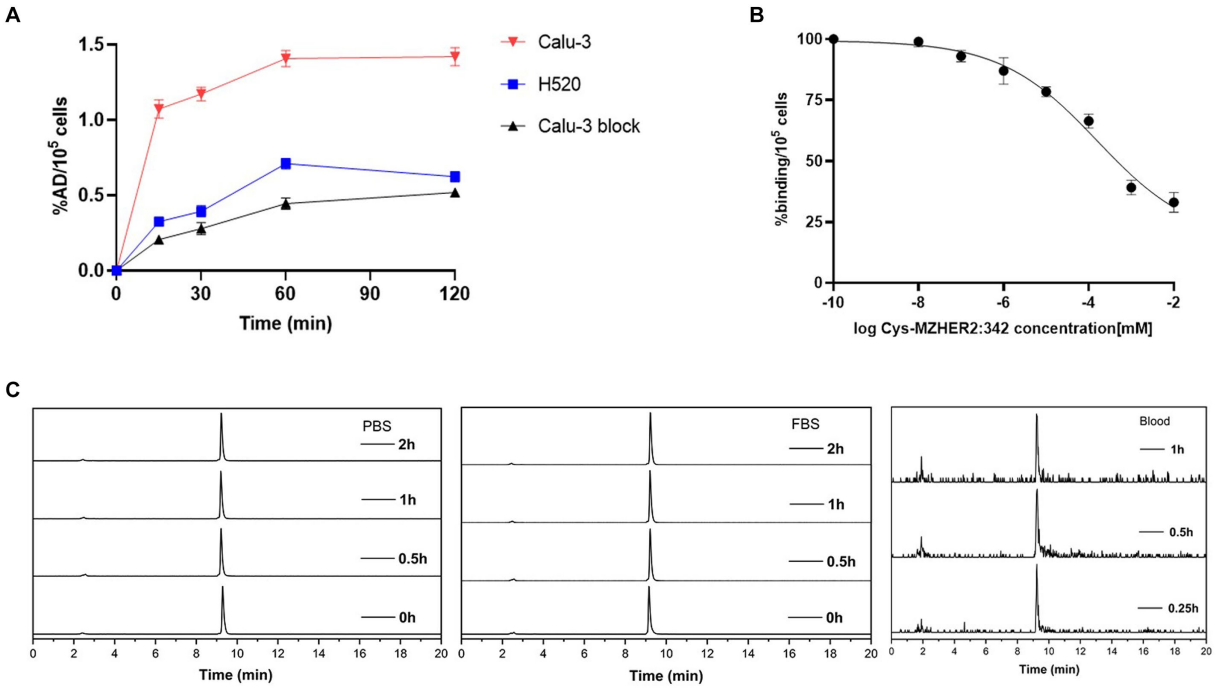


FIGURE 2
Cell uptake, cell binding, and stability of $^{68}$Ga-NOTA-MAL-Cys-MZHER$_{2:342}$. **(A)** Cell uptake of $^{68}$Ga-NOTA-MAL-Cys-MZHER$_{2:342}$ in Calu-3 and NCI-H520 cell lines. **(B)** Competitive cell binding assay of $^{68}$Ga-NOTA-MAL-Cys-MZHER$_{2:342}$ in Calu-3 cells. **(C)** HPLC chromatographic profiles of $^{68}$Ga-NOTA-MAL-Cys-MZHER$_{2:342}$ following *in vitro* and *in vivo* experimental procedures.

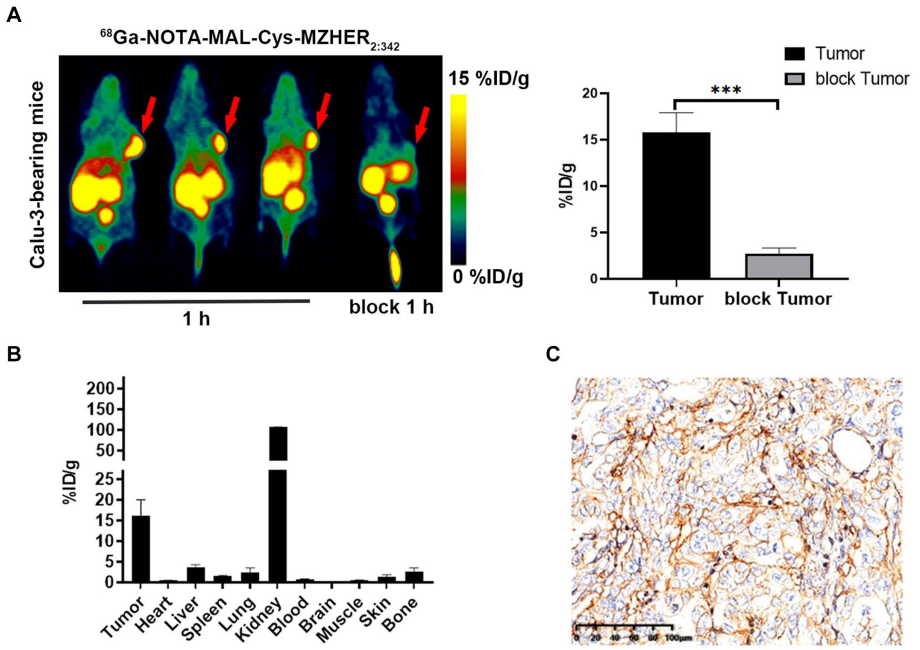


FIGURE 3
MicroPET imaging and biodistribution studies of $^{68}$Ga-NOTA-MAL-Cys-MZHER$_{2:342}$ in a xenograft model. **(A)** Whole-body microPET images ($n = 3$) of HER2-positive Calu-3-bearing mice, including blocking experiments with excess unlabeled Cys-MZHER$_{2:342}$. **(B)** Decay-corrected biodistribution of $^{68}$Ga-NOTA-MAL-Cys-MZHER$_{2:342}$ in tumor, heart, liver, spleen, lung, kidney, blood, and muscle tissues ($n = 3$). **(C)** Immunohistochemical analysis (20× magnification) of tumor tissues using HER2-specific antibodies. ***$p < 0.001$.

illustrated in Figure 4, both tracers exhibited uptake at tumor sites in the two patients, demonstrating favorable tumor-to-background ratios. Patient 1, 1-year post-primary resection for LUAD, displayed $^{68}$Ga-NOTA-MAL-Cys-MZHER$_{2:342}$ SUVmax values of 9.6 ± 0.5, 6.0 ± 0.3, and 2.5 ± 0.1 in mediastinal lymph nodes, left pleura, and L2 spine, respectively. Comparatively, the corresponding $^{18}$F-FDG SUVmax values

were 6.8 ± 0.2, 7.5 ± 0.3, and 6.3 ± 0.3. Concurrently, the liver exhibited an abnormal SUVmax value of 6.4 ± 0.4. In Patient 2, $^{68}$Ga-NOTA-MAL-Cys-MZHER$_{2:342}$ PET/CT imaging revealed primary and multiple metastatic foci (Figure 4B). The SUVmax values for the right lung upper lobe, left scapula, and subcarinal lymph nodes (NO. 7) were 7.3 ± 0.3, 3.1 ± 0.2, and 4.9 ± 0.2, respectively. The corresponding $^{18}$F-FDG SUVmax values were 16.6 ± 0.7, 10.9 ± 0.5, and 6.6 ± 0.3. Immunohistochemical analysis was performed on biopsy samples obtained from the primary tumor tissue of both patients. As depicted in Figure 4C, patient 1's biopsy sample scored HER2 3+, while patient 2 scored 1+.

TABLE 1 Biodistribution of $^{68}$Ga-NOTA-MAL-Cys-MZHER$_{2:342}$ in Calu-3-bearing mice.

| Organ (%ID/g) | 60 min |
|---|---|
| Tumor | 16.11 ± 3.91 |
| Heart | 0.50 ± 0.03 |
| Liver | 3.55 ± 0.73 |
| Spleen | 1.47 ± 0.25 |
| Lung | 2.44 ± 1.07 |
| Kidney | 106.85 ± 0.61 |
| Blood | 0.67 ± 0.20 |
| Brain | 0.08 ± 0.02 |
| Muscle | 0.46 ± 0.14 |
| Skin | 1.43 ± 0.39 |
| Bone | 3.00 ± 0.84 |
| **Ratios** | |
| Tumor/blood | 24.29 ± 1.93 |
| Tumor/muscle | 35.77 ± 2.14 |

## Discussion

Affibody molecules, small engineered scaffold proteins comprising 58 amino acids, are extensively utilized for binding to target proteins. These molecules are employed in tumor diagnosis and therapy due to their high affinity for molecular recognition (29, 30). To date, a variety of radiolabeled HER2 affibody molecules have been developed to image HER2 in tumors. A HER2-binding affibody, ZHER$_{2:342}$, has been screened and evaluated in preclinical and clinical PET studies (20, 23, 25). Different radioisotopes ($^{68}$Ga, $^{18}$F) labeled ZHER$_{2:342}$ and its analogs have demonstrated favorable performance in PET imaging. In our laboratory, $^{68}$Ga-NOTA-MAL-Cys-MZHER$_{2:342}$ is synthesized and prepared within 30 min, maintaining high radiolysis purity without further purification. Preliminary studies have shown satisfactory sensitivity and specificity in PET imaging of HER2-positive breast and gastric cancers with good contrast (22, 23). The application of $^{68}$Ga-NOTA-MAL-Cys-MZHER$_{2:342}$ to HER2-positive LC has not been evaluated until now. This study conducted evaluations of $^{68}$Ga-NOTA-MAL-Cys-MZHER$_{2:342}$ *in vitro*, *in vivo*, and in clinical patients with HER2-positive LUAD.

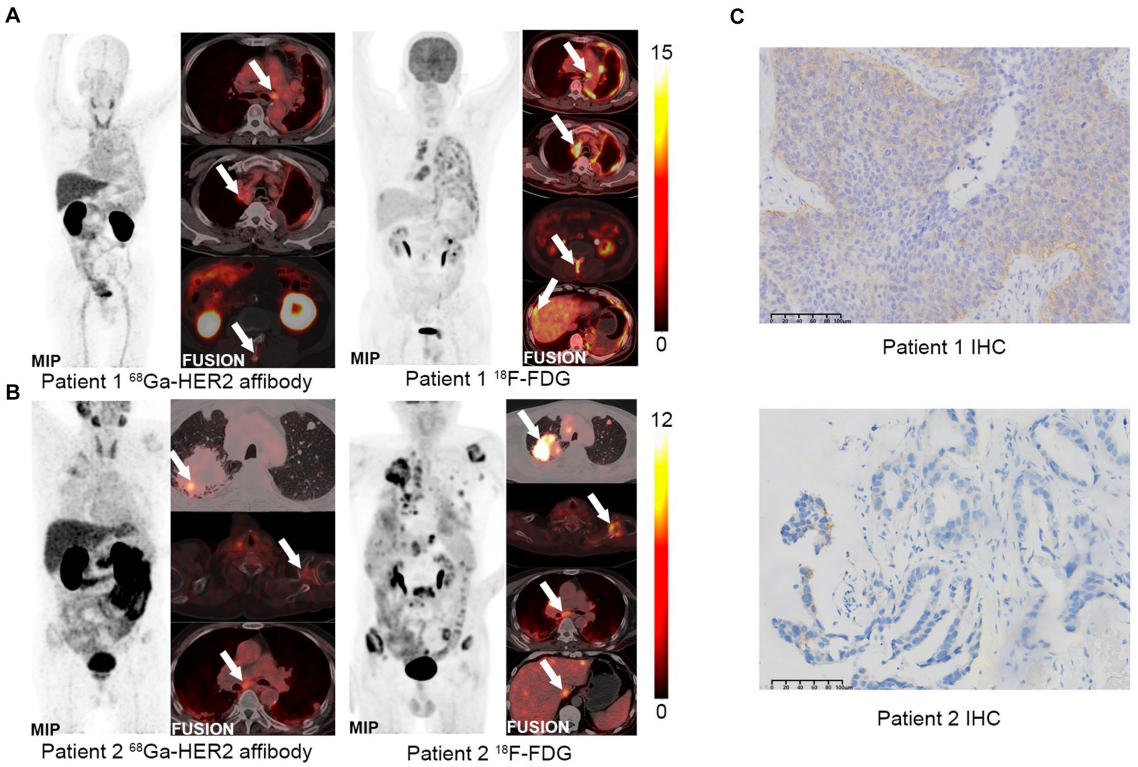


FIGURE 4
PET imaging of clinical patients using $^{68}$Ga-NOTA-MAL-Cys-MZHER$_{2:342}$. **(A,B)** Whole-body PET images of HER2-positive LUAD patients using $^{68}$Ga-NOTA-MAL-Cys-MZHER$_{2:342}$ and $^{18}$F-FDG, respectively. **(C)** Immunohistochemical analysis (20× magnification) of tumor tissues using HER2-specific antibodies.

Calu-3 cells, exhibiting high HER2 expression, were selected as positive cells, while NCI-H520 cells served as a negative control. In cell uptake experiments, NOTA-MAL-Cys-MZHER$_{2:342}$ was labeled with $^{68}$Ga and cultured with cells for 2 h. The results demonstrated high uptake in Calu-3 cells and low uptake in NCI-H520 cells. The addition of unlabeled Cys-MZHER$_{2:342}$ significantly decreased uptake in Calu-3 cells. The competitive binding assay revealed an $IC_{50}$ of 158.9 ± 1.73 nM for this tracer, comparable to other HER2-targeting tracers ($IC_{50}$ = 116.71 ± 1.28 nM) (25). The tracer also exhibited excellent stability under *in vitro* and *in vivo* conditions. In microPET imaging of xenograft models, ROI data indicated that $^{68}$Ga-NOTA-MAL-Cys-MZHER$_{2:342}$ exhibited higher radioactivity levels in Calu-3 tumors than other healthy organs, except for the kidney. The uptake values were notably higher than those observed with $^{99m}$Tc-Z$_{HER2:V2}$-pemetrexed (16.11 ± 3.91 %ID/g versus 2.6 ± 1.0 %ID/g) (18).

The diagnosis of tumor subtypes has traditionally relied on puncture biopsies, which are subject to high heterogeneity and dynamic expression, resulting in variable accuracy. Recent studies have demonstrated that misdiagnosis of HER2-positive breast cancer patients may occur when evaluating the efficacy of ADC drugs (31). Moreover, invasive puncture biopsies are not suitable for all patients. These limitations can be overcome by non-invasive PET/CT molecular imaging, which allows for the quantification of HER2 expression. While $^{18}$F-FDG, a glucose analog, plays a crucial role in detecting tissue metabolism, its utility in LC detection is limited. Studies have reported false positives in lymphoid follicles and pulmonary sclerosing hemangioma (32, 33). In contrast, HER2 receptor expression is typically minimal or absent in normal tissues. Compared to $^{18}$F-FDG, $^{68}$Ga-NOTA-MAL-Cys-MZHER$_{2:342}$ provides a clearer visualization of HER2 expression in both primary and metastatic lesions, offering significant value in selecting individualized treatment regimens and assessing efficacy.

The *in vivo* results prompted further evaluation of $^{68}$Ga-NOTA-MAL-Cys-MZHER$_{2:342}$ PET imaging in two patients with HER2-positive LUAD. The imaging demonstrated satisfactory tumor uptake and rapid clearance from normal organs, indicating high sensitivity and specificity in binding to HER2-positive LUAD cells. Notably, patient 2 exhibited negative IHC results; however, HER2 affibody PET/CT revealed high uptake, which was subsequently confirmed as HER2 amplification through genetic testing. This finding further underscores the importance of $^{68}$Ga-NOTA-MAL-Cys-MZHER$_{2:342}$ in diagnosing HER2 expression levels in LC. This case emphasizes the potential of 68Ga-NOTA-MAL-Cys-MZHER$_{2:342}$ as a valuable diagnostic tool, particularly in cases where traditional methods fail. The ability to identify HER2-positive lesions accurately can significantly impact treatment decisions, as patients with HER2-positive lesions are more likely to benefit from targeted therapies such as trastuzumab and other HER2 inhibitors. Furthermore, the use of PET/CT imaging can guide biopsy locations, ensuring that samples are taken from areas with the highest tracer uptake, thus improving the likelihood of detecting HER2-positive.

Despite its high sensitivity and specificity for HER2-positive LUAD, increased tracer accumulation was observed in the kidney and liver. This accumulation may present challenges in assessing patients with distant metastases. In the clinical evaluation of LC patients, the tracer was unable to detect metastases due to high renal metabolism. This contrasts with $^{18}$F-FDG, which successfully located corresponding areas of high metabolism (Figures 4A,B). Previous research has reported that HER2 affibody modified by an enzymolysis clearance strategy can effectively reduce renal uptake (34). This approach may offer a promising solution for reducing the non-tumor uptake of $^{68}$Ga-NOTA-MAL-Cys-MZHER$_{2:342}$.

## Conclusion

In conclusion, $^{68}$Ga-NOTA-MAL-Cys-MZHER$_{2:342}$ exhibits exceptional performance in both *in vitro* and *in vivo* models, as well as in clinical patients. This novel radiotracer holds significant potential for contributing to personalized clinical diagnosis and treatment strategies in the future.

## Data availability statement

The raw data supporting the conclusions of this article will be made available by the authors, without undue reservation.

## Ethics statement

The studies involving humans were approved by the Ethics Committee of the Peking University Cancer Hospital (NCT04547309). The studies were conducted in accordance with the local legislation and institutional requirements. The participants provided their written informed consent to participate in this study. The animal study was approved by the Animal Research Committee of Jiangsu Institute of Atomic Medicine. The study was conducted in accordance with the local legislation and institutional requirements. Written informed consent was obtained from the individual(s) for the publication of any potentially identifiable images or data included in this article.

## Author contributions

SL: Conceptualization, Data curation, Writing – original draft, Writing – review & editing. KW: Conceptualization, Writing – review & editing, Writing – original draft. XZ: Methodology, Software, Validation, Writing – original draft, Writing – review & editing. DP: Resources, Writing – review & editing. LW: Data curation, Validation, Writing – review & editing. XGu: Data curation, Software, Writing – review & editing. XGa: Formal analysis, Validation, Writing – review & editing. QL: Formal analysis, Validation, Writing – review & editing. XW: Project administration, Writing – review & editing, Writing – original draft.

## Funding

The author(s) declare that financial support was received for the research, authorship, and/or publication of this article. This article was supported by the Project of Jiangsu Commission of Health (H2023150), the Top Talent Support Program for young and middle-aged people of Wuxi Health Committee (BJ2020025, BJ2023030), the Major Project of Wuxi Municipal Health Commission (Z202303, Z202009), the Scientific Research Program of Wuxi Health

Commission (MS20193e7, T201937), and China Postdoctoral Science Foundation (2020M670069ZX).

## Conflict of interest

The authors declare that the research was conducted in the absence of any commercial or financial relationships that could be construed as a potential conflict of interest.

## Publisher's note



## References

1. Sung H, Ferlay J, Siegel RL, Laversanne M, Soerjomataram I, Jemal A, et al. Global cancer statistics 2020: Globocan estimates of incidence and mortality worldwide for 36 cancers in 185 countries. *CA Cancer J Clin*. (2021) 71:209–49. doi: 10.3322/caac.21660

2. Xia C, Dong X, Li H, Cao M, Sun D, He S, et al. Cancer statistics in China and United States, 2022: profiles, trends, and determinants. *Chin Med J*. (2022) 135:584–90. doi: 10.1097/cm9.0000000000002108

3. Tsao AS, Scagliotti GV, Bunn PA Jr, Carbone DP, Warren GW, Bai C, et al. Scientific advances in lung cancer 2015. *J Thorac Oncol*. (2016) 11:613–38. doi: 10.1016/j.jtho.2016.03.012

4. Swain SM, Shastry M, Hamilton E. Targeting Her2-positive breast cancer: advances and future directions. *Nat Rev Drug Discov*. (2023) 22:101–26. doi: 10.1038/s41573-022-00579-0

5. Digklia A, Wagner AD. Advanced gastric cancer: current treatment landscape and future perspectives. *World J Gastroenterol*. (2016) 22:2403–14. doi: 10.3748/wjg.v22.i8.2403

6. Ren S, Wang J, Ying J, Mitsudomi T, Lee DH, Wang Z, et al. Consensus for Her2 alterations testing in non-small-cell lung cancer. *ESMO Open*. (2022) 7:100395. doi: 10.1016/j.esmoop.2022.100395

7. Liu L, Shao X, Gao W, Bai J, Wang R, Huang P, et al. The role of human epidermal growth factor receptor 2 as a prognostic factor in lung cancer: a meta-analysis of published data. *J Thorac Oncol*. (2010) 5:1922–32. doi: 10.1097/jto.0b013e3181f26266

8. Tsurutani J, Iwata H, Krop I, Jänne PA, Doi T, Takahashi S, et al. Targeting Her2 with Trastuzumab Deruxtecan: a dose-expansion, phase I study in multiple advanced solid Tumors. *Cancer Discov*. (2020) 10:688–701. doi: 10.1158/2159-8290.Cd-19-1014

9. Le X, Cornelissen R, Garassino M, Clarke JM, Tchekmedyian N, Goldman JW, et al. Poziotinib in non-small-cell lung cancer Harboring Her2 exon 20 insertion mutations after prior therapies: Zenith20-2 trial. *J Clin Oncol*. (2022) 40:710–8. doi: 10.1200/jco.21.01323

10. Zhang S, Wang W, Xu C, Zhang Y, Cai X, Wang Q, et al. Chinese expert consensus on the diagnosis and treatment of Her2-altered non-small cell lung cancer. *Thorac Cancer*. (2023) 14:91–104. doi: 10.1111/1759-7714.14743

11. Almendro V, Marusyk A, Polyak K. Cellular heterogeneity and molecular evolution in cancer. *Annu Rev Pathol*. (2013) 8:277–302. doi: 10.1146/annurev-pathol-020712-163923

12. Foster B, Bagci U, Mansoor A, Xu Z, Mollura DJ. A review on segmentation of positron emission tomography images. *Comput Biol Med*. (2014) 50:76–96. doi: 10.1016/j.compbiomed.2014.04.014

13. Phelps ME. Molecular imaging with positron emission tomography. *Annu Rev Nucl Part Sci*. (2002) 52:303–38. doi: 10.1146/annurev.nucl.52.050102.090725

14. Shim SS, Lee KS, Kim BT, Choi JY, Chung MJ, Lee EJ. Focal parenchymal lung lesions showing a potential of false-positive and false-negative interpretations on integrated pet/Ct. *AJR Am J Roentgenol*. (2006) 186:639–48. doi: 10.2214/ajr.04.1896

15. Rubello D, Nanni C, Castellucci P, Rampin L, Farsad M, Franchi R, et al. Does 18f-Fdg pet/Ct play a role in the differential diagnosis of parotid masses. *Panminerva Med*. (2005) 47:187–9.

16. Woo SK, Jang SJ, Seo MJ, Park JH, Kim BS, Kim EJ, et al. Development of (64)cu-Nota-Trastuzumab for Her2 targeting: a radiopharmaceutical with improved pharmacokinetics for human studies. *J Nucl Med*. (2019) 60:26–33. doi: 10.2967/jnumed.118.210294

17. Paudyal P, Paudyal B, Hanaoka H, Oriuchi N, Iida Y, Yoshioka H, et al. Imaging and biodistribution of Her2/Neu expression in non-small cell lung cancer xenografts with cu-Labeled Trastuzumab pet. *Cancer Sci*. (2010) 101:1045–50. doi: 10.1111/j.1349-7006.2010.01480.x

18. Jiao H, Zhao X, Liu J, Ma T, Zhang Z, Zhang J, et al. In vivo imaging characterization and anticancer efficacy of a novel Her2 Affibody and Pemetrexed conjugate in lung cancer model. *Nucl Med Biol*. (2019) 68-69:31–9. doi: 10.1016/j.nucmedbio.2018.11.004

19. Han J, Zhao Y, Zhao X, Ma T, Hao T, Liu J, et al. Therapeutic efficacy and imaging assessment of the Her2-targeting chemotherapy drug Z(Her2:V2)-Pemetrexed in lung adenocarcinoma xenografts. *Investig New Drugs*. (2020) 38:1031–43. doi: 10.1007/s10637-019-00876-3

20. Kramer-Marek G, Kiesewetter DO, Martiniova L, Jagoda E, Lee SB, Capala J. [18f]Fbem-Z(Her2:342)-Affibody molecule-a new molecular tracer for in vivo monitoring of Her2 expression by positron emission tomography. *Eur J Nucl Med Mol Imaging*. (2008) 35:1008–18. doi: 10.1007/s00259-007-0658-0

21. Kramer-Marek G, Bernardo M, Kiesewetter DO, Bagci U, Kuban M, Aras O, et al. Pet of Her2-positive pulmonary metastases with 18f-Zher2:342 Affibody in a murine model of breast cancer: comparison with 18f-Fdg. *J Nucl Med*. (2012) 53:939–46. doi: 10.2967/jnumed.111.100354

22. Zhou N, Liu C, Guo X, Xu Y, Gong J, Qi C, et al. Impact of (68)Ga-Nota-mal-Mzher2 pet imaging in advanced gastric cancer patients and therapeutic response monitoring. *Eur J Nucl Med Mol Imaging*. (2021) 48:161–75. doi: 10.1007/s00259-020-04898-5

23. Xu Y, Wang L, Pan D, Yu C, Mi B, Huang Q, et al. Pet imaging of a (68)Ga Labeled modified Her2 Affibody in breast cancers: from xenografts to patients. *Br J Radiol*. (2019) 92:20190425. doi: 10.1259/bjr.20190425

24. Pan D, Liu G, Xu Y, Wang Y, Yue Y, Wang L, et al. Pet imaging of Fshr expression in Tumors with (68)Ga-Labeled Fsh1 peptide. *Contrast Media Mol Imaging*. (2017) 2017:2674502. doi: 10.1155/2017/2674502

25. Xu Y, Bai Z, Huang Q, Pan Y, Pan D, Wang L, et al. Pet of Her2 expression with a novel (18)Fal Labeled Affibody. *J Cancer*. (2017) 8:1170–8. doi: 10.7150/jca.18070

26. Kiesewetter DO, Guo N, Guo J, Gao H, Zhu L, Ma Y, et al. Evaluation of an [(18)F]Alf-Nota Analog of Exendin-4 for imaging of Glp-1 receptor in Insulinoma. *Theranostics*. (2012) 2:999–1009. doi: 10.7150/thno.5276

27. Xu Q, Zhu C, Xu Y, Pan D, Liu P, Yang R, et al. Preliminary evaluation of [18f]Alf-Nota-mal-Cys39-Exendin-4 in Insulinoma with pet. *J Drug Target*. (2015) 23:813–20. doi: 10.3109/1061186x.2015.1020808

28. Yu C, Pan D, Mi B, Xu Y, Lang L, Niu G, et al. (18)F-Alfatide ii pet/Ct in healthy human volunteers and patients with brain metastases. *Eur J Nucl Med Mol Imaging*. (2015) 42:2021–8. doi: 10.1007/s00259-015-3118-2

29. Akbari V, Chou CP, Abedi D. New insights into affinity proteins for Her2-targeted therapy: beyond Trastuzumab. *Biochim Biophys Acta Rev Cancer*. (2020) 1874:188448. doi: 10.1016/j.bbcan.2020.188448

30. Eissler N, Altena R, Alhuseinalkhudhur A, Bragina O, Feldwisch J, Wuerth G, et al. Affibody pet imaging of Her2-expressing cancers as a key to guide Her2-targeted therapy. *Biomedicines*. (2024) 12:1088. doi: 10.3390/biomedicines12051088

31. Modi S, Jacot W, Yamashita T, Sohn J, Vidal M, Tokunaga E, et al. Trastuzumab Deruxtecan in previously treated Her2-low advanced breast cancer. *N Engl J Med*. (2022) 387:9–20. doi: 10.1056/NEJMoa2203690

32. Chung JH, Cho KJ, Lee SS, Baek HJ, Park JH, Cheon GJ, et al. Overexpression of Glut1 in lymphoid follicles correlates with false-positive (18)F-Fdg pet results in lung cancer staging. *J Nucl Med*. (2004) 45:999–1003.

33. Lee E, Park CM, Kang KW, Goo JM, Kim MA, Paeng JC, et al. 18f-Fdg pet/Ct features of pulmonary sclerosing hemangioma. *Acta Radiol*. (2013) 54:24–9. doi: 10.1258/ar.2011.110474

34. Zhang M, Kang F, Xing T, Wang J, Ma T, Li G, et al. First-in-human validation of Enzymolysis clearance strategy for decreasing renal radioactivity using modified [(68)Ga]Ga-Her2 Affibody. *Eur J Nucl Med Mol Imaging*. (2024) 51:1713–24. doi: 10.1007/s00259-023-06584-8